ACS OMEGA

http://pubs.acs.org/journal/acsodf

Article

Effect of SiO_2@PEGMA Composites on Mechanical Properties of Oil Well Cement

Gang Wang,* Hua Tan,* Chunjing Lu, and Ao Sun

Cite This: *ACS Omega* 2022, 7, 24012−24019

Read Online

ACCESS | Metrics & More | Article Recommendations

ABSTRACT: SiO_2@PEGMA composites were synthesized by grafting poly(ethylene glycol) methacrylate (PEGMA) on SiO_2 nanoparticles via radical polymerization. The chemical structures of the SiO_2@PEGMA composites were analyzed by Fourier transform infrared, ^1H NMR, and transmission electron microscopy methods. The mechanical and fresh properties, hydration products, heat of hydration, microtopography, and pore structures were studied. The shell formed by the grafted PEGMA gave the SiO_2@PEGMA composite a steric hindrance effect, which enabled it to have excellent dispersion stability even in the cement pore solution. The SiO_2@PEGMA composites could not only effectively facilitate hydration reaction and generate calcium silicate hydrate (C−S−H) through the seeding effect but also make the pore structure more compact by the filling effect. Compared with other control groups, SiO_2@PEGMA composites could obviously enhance the compressive strength of cement samples, which was increased by 36.7% after curing for 28 days.

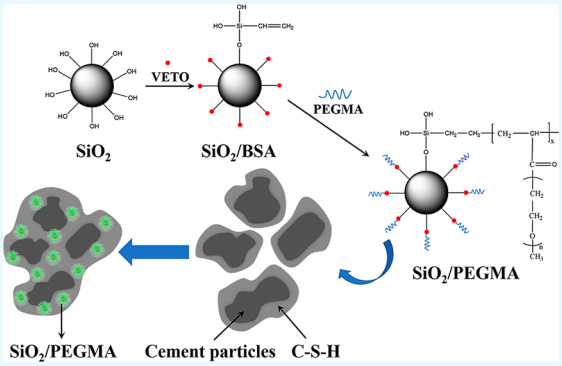

1. INTRODUCTION

After the cementing operation, hardened cement pastes are required to effectively isolate the pay zone and provide protection and support for the casing, which is very important for oilfield development.[1−3] The safety and quality of cementing construction mainly depend on the performance of oil well cement.[4,5] Because cement is a brittle material, it is easy to produce micro-cracks and micro-annuli due to the subsequent operations such as perforation, fracturing, and the complex forces of underground rock formations, resulting in the failure of interlayer isolation between oil wells, which is not conducive to oilfield development.[6−9] Cementing is complex and challenging due to the intricacy of the geological conditions of the target layer.

Nanomaterials have been shown to affect the hydration process of cement through their unique physicochemical properties, thereby fundamentally affecting the macroscopic properties of oil well cement.[10−12] At present, more and more nanomaterials are used to modify oil well cement, such as SiO_2 nanoparticles,[13] TiO_2 nanoparticles,[14] Fe_2O_3 nanoparticles,[15] Al_2O_3 nanoparticles, and[16] nano clay.[17] Among them, nano-SiO_2 is a kind of nanomaterial studied earlier and is most widely used in cement.[18−20] Compared with other nanomaterials, SiO_2 nanoparticles can not only play a physical filling role but also generate C−S−H via reacting with $Ca(OH)_2$, thereby promoting the hydration process, densifying the microstructure, and improving the macroscopic properties of cement.[21−23] However, SiO_2 nanoparticles have extremely high surface energy and can easily agglomerate in cement pore solution, which reduces their efficacy significantly, and their application in cementing is limited.[24] The strong agglomeration tendency of SiO_2 nanoparticles is hindered by adding polymeric dispersants in cementing. Polyether-based, polycarboxylate, and phosphate superplasticizers are commonly used superplasticizers.[25,26] The polycarboxylate superplasticizer is the most widely used, and it can not only adsorb SiO_2 nanoparticles to improve their dispersion stability but also adsorb cement particles to promote cement hydration.[27−29] However, SiO_2 nanoparticles as inorganic particles are difficult to make compatible with organic polymers by physical blending, which makes the agglomeration of SiO_2 nanoparticles not effectively solved.[30] Besides, the polycarboxylate superplasticizers delay the hydration process and reduce the early compressive strength of hardened cement pastes, which is harmful to the compressive strength of cement.[31]

Inorganic particles with grafted polymers can produce synergistic effects to impart the composites with unique functionalities, so they have great application potential as multifunctional materials.[32,33] Through the formation of chemical bonds, the interaction between polymers and SiO_2

Received: May 23, 2022
Accepted: June 22, 2022
Published: June 30, 2022

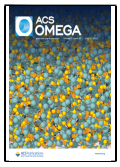

© 2022 The Authors. Published by American Chemical Society

nanoparticles is strong, and the agglomeration or secondary agglomeration is not easy to occur. Hence, the composite material can avoid the occurrence of phase separation.[34−37] In addition, introducing a polymer into the SiO_2 nanoparticles can produce a synergistic effect, showing excellent performance in mechanical properties, thermals, optics, and electricity.[38−40] The SiO_2 nanoparticles with the grafted polymer can effectively improve their dispersion stability, which may benefit the performance of oil well cement.

In this paper, SiO_2@PEGMA composites were produced by grafting poly(ethylene glycol) methacrylate (PEGMA) on the SiO_2 nanoparticles via radical polymerization. The impacts of the SiO_2@PEGMA composites on mechanical properties, fresh properties, and the hydration process of cement were researched. Hydration products, micromorphology, and pore structures of cement were characterized to analyze the enhancement mechanism of the mechanical properties by nanoindentation, BES-scanning electron microscopy (SEM), and MIP, respectively.

2. EXPERIMENTAL SECTION

2.1. Materials. Anhydrous ethanol, calcium hydroxide, and potassium hydroxide were supplied from the Damao Chemical Reagent Co. Ltd., Tianjin, China. Fumed silica nanoparticles (SiO_2 nanoparticles, 50 nm), PEGMA, triethoxyvinylsilane (VTEO), and ammonium persulfate (APS) were supplied from the Aladdin Reagent Co., Ltd., Shanghai, China. The polycarboxylic superplasticizer (PEGMA/AA) was provided by SinoPec Shengli Petroleum Engineering Co. Ltd., Dongying, China. Class G oil well cement was obtained from Jiahua Special Cement Co., Ltd., Leshan, China. The composition of the oil well cement is displayed in Table 1.

Table 1. Chemical Compositions of the Oil Well Cement (%)

SiO_2	Al_2O_3	Fe_2O_3	CaO	MgO	K_2O	SO_3	MnO_2	loss on ignition
24.5	3.7	3.8	61.6	2.2	0.2	2.3	0.2	1.5

2.2. Preparation of SiO_2@PEGMA. 3% VTEO was stirred in water for 2 h for the hydrolysis reaction. 1% SiO_2 nanoparticles were ultrasonically dispersed in 20% ethanol solution and mixed with the VTEO solution mentioned above. The suspension was agitated at 45 °C for 8 h under nitrogen. After the reaction was completed, it was cooled, centrifuged, and washed three times with anhydrous ethanol to remove the VTEO that was not grafted on the SiO_2 nanoparticles. The product (SiO_2−VTEO) was dried at 80 °C for 24 h.

After dispersing 1% SiO_2−VTEO in absolute ethanol, 0.015% APS and 4% PEGMA were mixed, and the mixture was stirred at 60 °C for 6 h under nitrogen. The product was then centrifuged and washed, and the obtained target product was labeled as SiO_2@PEGMA composites, and their preparation principle is shown in Figure 1.

2.3. Preparation of Cement Samples. The cement pastes with a water−cement ratio of 0.44 cured at 75 °C were prepared to analyze the influence of the additives on oil well cement, including reference cement, cement containing SiO_2 nanoparticles, cement containing 0.3% PEGMA/AA superplasticizer and SiO_2 nanoparticles, and cement containing SiO_2@PEGMA composites. Moreover, the four kinds of cement samples were labeled as a reference, SiO_2, SiO_2 + P, and SiO_2@PEGMA, respectively.

2.4. Particle Size Distributions. The SiO_2 nanoparticles and SiO_2@PEGMA composites were dispersed in distilled water, 0.4 M KOH, and saturated calcium hydroxide solution by ultrasonic dispersion for 5 min, respectively. The cumulative particle size distributions were determined by dynamic light scattering (DynaPro NanoStar, USA) after standing for 1 h.

2.5. Compressive Strength. The cement pastes at a water-to-cement ratio of 0.44 were injected into a 50.8 mm cube mold and cured at 75 °C for 3, 7, and 28 days, respectively. The compressive strength of the hardened cement paste was measured using a cement pressure tester (YAW-300C, China) at a loading rate of 72 kN/min. Five tests were conducted to determine the compressive strength of each cement sample at each curing period.

2.6. Slump. The slump of the cement slurries was tested using a truncated metal cone (an upper port diameter of 36 mm, a lower port diameter of 60 mm, and a height of 60 mm). The cement slurry was poured into the truncated metal cone, placed on a horizontal glass plate, and leveled with a scraper to make the slurry flush with the upper opening of the circular mold. The truncated cone was lifted vertically, and the maximum diameter of the flowing cement slurry was measured after 30 s.

2.7. Nanoindentation. A nanoindenter (TI-950, USA) was applied for nanoindentation analysis on the polished surface of cement samples. The specimens were sliced thin to

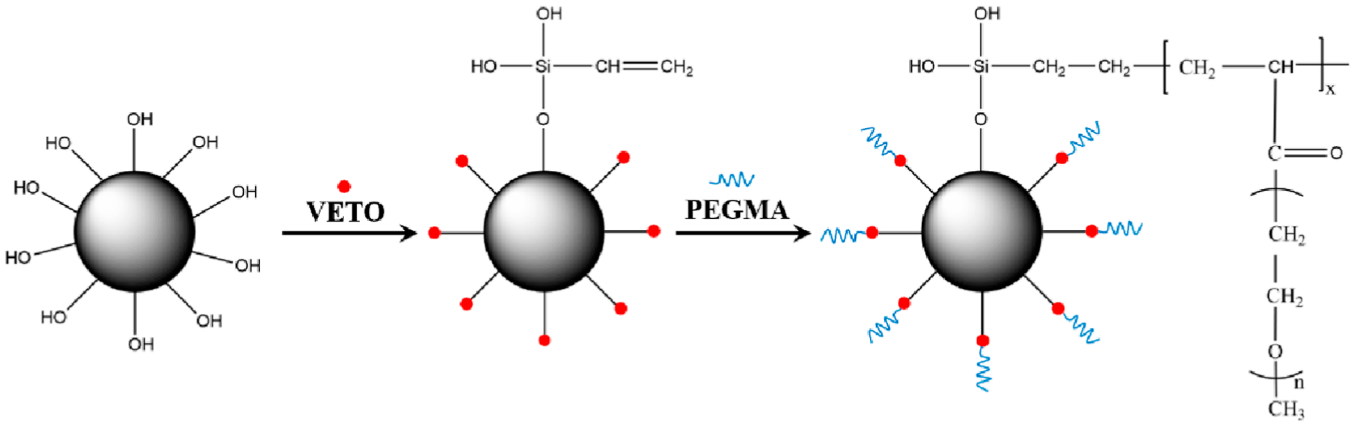

Figure 1. Preparation principle of SiO_2@PEGMA composites.

https://doi.org/10.1021/acsomega.2c03202
ACS Omega 2022, 7, 24012−24019

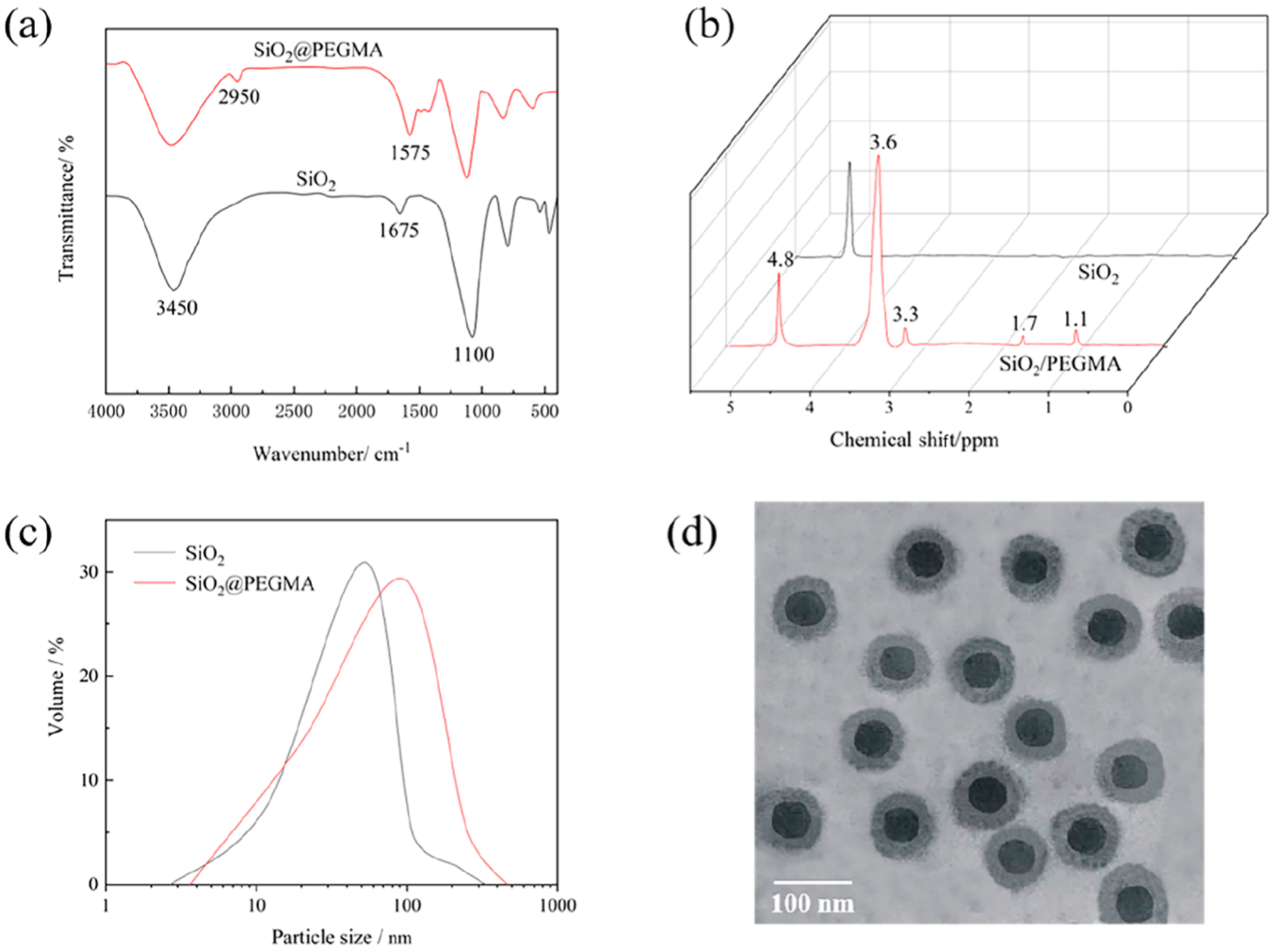

Figure 2. FTIR spectra of SiO_2 and SiO_2@PEGMA (a); ^1H NMR spectra of SiO_2 and SiO_2@PEGMA (b); particle size distribution of SiO_2 and SiO_2@PEGMA (c); and TEM of SiO_2@PEGMA (d).

prepare polished sections. For the polishing stage, silicon carbide paper and an automatic polishing machine with a gradation of 1 μm were used.

2.8. Test Methods. Fourier transform infrared (FTIR) spectrometry and ^1H NMR spectroscopy were used to characterize the chemical structure of SiO_2@PEGMA composites and SiO_2 nanoparticles. Dynamic light scattering (DynaPro NanoStar, USA) was applied to analyze the particle size distribution of SiO_2@PEGMA composites and SiO_2 nanoparticles after ultrasonic dispersion for 5 min. Transmission electron microscopy (TEM, JEOL 2010, Japan) was applied to observe the core−shell structure of SiO_2@PEGMA composites. An isothermal calorimeter (I-Cal 4000 HPC, China) was utilized to monitor the heat of hydration of cement within 72 h. The backscattered electron model of a scanning electron microscope (SU3800, Japan) was used to observe the polished surfaces of hardened cement pastes after curing for 3 days. After 3 days of curing, the pore structure of cement samples was analyzed using a mercury intrusion porosimeter (AutoPore III, USA).

3. RESULTS AND DISCUSSION

3.1. Characterization of SiO_2@PEGMA. The FTIR was used to determine the chemical composition of the SiO_2@PEGMA composites and SiO_2 nanoparticles. As shown in Figure 2a, the peaks at 1100, 1675, and 3450 cm^{-1} correspond to the bands of the Si−O−Si, H_2O, and Si−OH in the SiO_2 nanoparticles. For the SiO_2@PEGMA composites, there were peaks of C═O and C−H at 1575 and 2950 cm^{-1}, respectively, which verified that PEGMA had been successfully grafted on the SiO_2 nanoparticles. ^1H NMR was used further to confirm the chemical structures of the SiO_2@PEGMA composites. As shown in Figure 2b, the chemical shift value at 4.8 ppm was contributed by the adsorbed water. For the SiO_2@PEGMA composites, the peaks centered at 1.1 and 1.7 ppm were the stretching vibrations of the $-CH_3$ and $-CH_2$, respectively. Additionally, the peaks at 3.3 and 3.6 ppm correspond to the $O-CH_3$ and $-CH_2-CH_2-O$. The characteristic peaks appeared in SiO_2@PEGMA composites, which further indicated that the objective composites had been prepared. As shown in Figure 2c, SiO_2@PEGMA composites with the shell structure had a broader particle size distribution and a rise in average particle size from 54 to 90 nm when compared with SiO_2 nanoparticles. As seen in Figure 2d, the core−shell structure of the SiO_2@PEGMA composite was clearly visible. The shells formed by PEGMA with a thickness of about 18 nm uniformly covered the SiO_2 nanoparticles.

3.2. Particle Size Distribution Analysis. Cumulative particle size distributions of SiO_2 nanoparticles before and after modification dispersed in deionized water, potassium hydrox-

https://doi.org/10.1021/acsomega.2c03202
ACS Omega 2022, 7, 24012−24019

ide solution, and calcium hydroxide saturated solution were presented in Figure 3. The cumulative particle size distribution

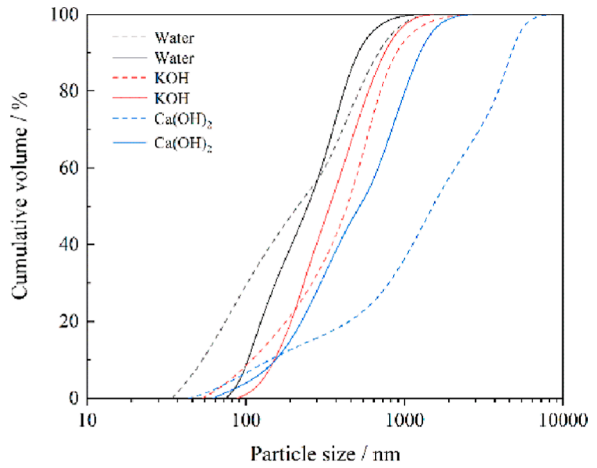

Figure 3. Accumulated curves of SiO_2@PEGMA composites (full lines) and SiO_2 nanoparticles (dashed) dispersed in deionized water, KOH solution, and $Ca(OH)_2$ saturated solution.

of SiO_2@PEGMA composites in the above solutions was narrower, although the grafted PEGMA increased the nanoparticle size. Compared with deionized water, the cumulative particle size distribution of SiO_2 nanoparticles in the potassium hydroxide solution varied slightly. This was mainly due to the electrostatic repulsion generated by the $Si-O^-$ on the surface of SiO_2 nanoparticles under alkaline conditions, which played a role in stabilizing the nanoparticles. However, the cumulative particle size distributions of SiO_2 nanoparticles were obviously shifted to the right and broadened in $Ca(OH)_2$ saturated solution, mainly due to the decrease in electrostatic repulsion caused by the adsorption of Ca^{2+}. There was no significant difference in the cumulative particle size distribution of SiO_2@PEGMA composites in the above solutions. The results showed that compared with SiO_2 nanoparticles, SiO_2@PEGMA composites had higher stability in calcium hydroxide saturated solution. This was because the van der Waals attraction between composites was overcome by the steric hindrance effect created by the PEGMA shell, which improved the stab dispersion stability of SiO_2@PEGMA composites.

3.3. Mechanical Properties. The compressive strength of hardened cement pastes with different SiO_2@PEGMA dosages after curing for 3 days was displayed in Figure 4a. With the higher dosages of SiO_2@PEGMA composites, the compressive strength of cement samples increased until it reached 39.8 MPa at 2 wt %. The compressive strengths of cement samples with curing times of 3, 7, and 28 days are illustrated in Figure 4b. As a reference, SiO_2, SiO_2 + P, and SiO_2@PEGMA represented oil well cement without additives, with 2 wt % SiO_2 nanoparticles, with 0.3 wt % PEGMA/AA superplasticizer and 2 wt % SiO_2 nanoparticles, and with 2 wt % SiO_2@PEGMA composites, respectively. Due to the steady progression of the hydration reaction, the compressive strength of each cement sample rose with curing time. Among all cement samples, SiO_2@PEGMA had the largest compressive strength at each curing time. Compared with the reference, the compressive strengths of SiO_2, SiO_2 + P, and SiO_2@PEGMA with a curing time of 28 days improved by 8.7, 16.2, and 36.7%, respectively. Ideally, the cement pore solution was considered a $Ca(OH)_2$ saturated solution. In this environment, it was challenging to maintain the stable dispersion of nanoparticles only through the Derjaguin−Landau−Verwey−Overbeek interaction. Providing additional surface repulsion by steric hindrance was beneficial to improving the dispersion stability of nanoparticles. The steric hindrance repulsive force provided by the PEGMA shell of SiO_2@PEGMA composites was the main driving force for good dispersion. The SiO_2@PEGMA composites with excellent dispersibility could exert the seeding effect, which closely relied on the specific surface area of the nanoparticles. The SiO_2@PEGMA composites absorb or react with Ca^{2+} to generate nucleation sites, promoting the hydration reaction to improve the mechanical properties effectively.

3.4. Fresh Properties. The fresh properties of cement slurries are given in Table 2. According to the on-site construction requirements, the slump of the cement slurry should be at least greater than 200 mm, and the ideal slump range should be between 220 and 240 mm.[41] The results showed that the slump of the four kinds of cement slurries met the requirements, but the cement slurry slump of SiO_2 + P and SiO_2@PEGMA was more suitable. The fresh density of cement

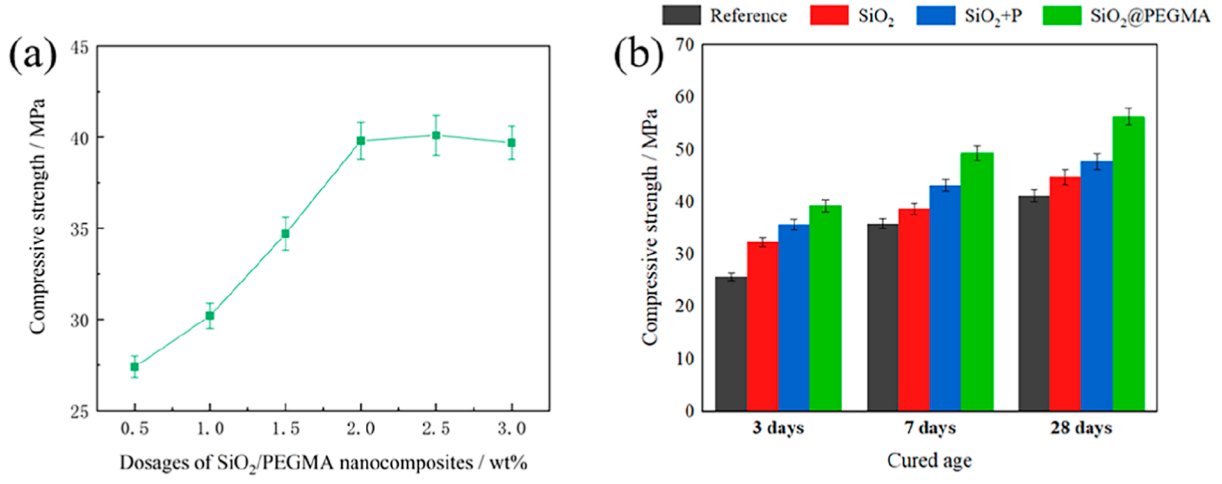

Figure 4. Compressive strength of hardened cement pastes changed with the dosages of SiO_2@PEGMA composites (a) and compressive strength of the four kinds of cement samples (b).

https://doi.org/10.1021/acsomega.2c03202
ACS Omega 2022, 7, 24012−24019

Table 2. Pore Structure Parameters of Cement Samples

cement samples	slump/mm	fresh density/(kg/m^3)	bleeding/mL
reference	216	1862	0
SiO_2	209	1873	0
SiO_2 + P	236	1876	0
SiO_2@PEGMA	231	1877	0

slurries was in the range of 1862−1877 kg/m^3 with no apparent difference. At the same time, according to the performance requirements of oil well cement, the bleeding of the cement slurries should be zero, and the above four kinds of cement slurries could be used in oil well cementing construction.

3.5. Nanoindentation. The probability density function of the indentation modulus of the polished cement samples was shown in Figure 5. Four identified phases of the nanoindentation experiment were considered calcium hydroxide (CH), high-density C−S−H (HD C−S−H), low-density C−S−H (LD C−S−H), and loose-packed C−S−H (LP C−S−H) in descending order. HD C−S−H and LD C−S−H could improve the compressive strengths of cement samples, while LP C−S−H was predominated by pores, which detrimentally affected the macroscopic properties of cement.[42,43] From Figure 5a,b, the fraction of LD C−S−H, HD C−S−H, and CH of the cement samples increased, while the fraction of LP C−S−H decreased. Among all cement samples, SiO_2@PEGMA cement had the highest fraction of HD C−S−H, LD C−S−H, and CH and the lowest fraction of LP C−S−H. The results showed that SiO_2@PEGMA composites could more effectively improve the hydration reaction and enhance the mechanical properties of cement.

3.6. Isothermal Calorimetry Analysis. The heat of hydration of cement is shown in Figure 6. Compared with the reference, the hydration heat of the cement containing SiO_2 nanoparticles changed slightly, while that of the cement containing SiO_2 + P increased appreciably, reaching a peak value of 3.82 mW/g. The SiO_2@PEGMA composites had the most obvious influence on promoting heat of hydration; not only was the initial acceleration time the earliest but also the peak value was as high as 4.07 mW/g. The seeding effect of nanoparticles can accelerate the hydration process, which significantly reduces when the nanoparticles agglomerate.[44] Compared with SiO_2 and SiO_2 + P, the PEGMA shell of SiO_2@PEGMA composites could markedly boost the dispersion stability by the steric hindrance repulsive force, which was beneficial for their seeding effect to promote the cement hydration effectively.

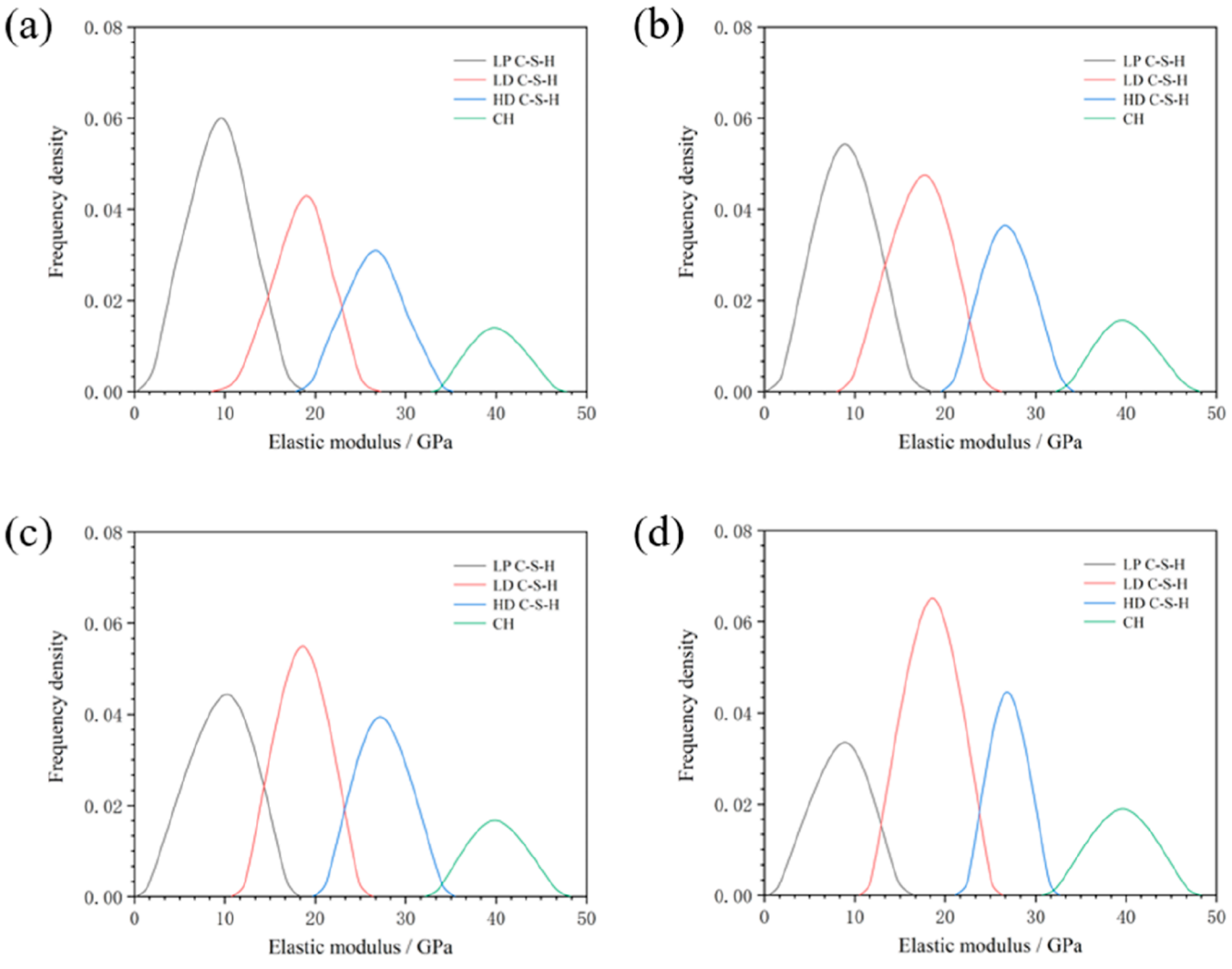

Figure 5. Modulus probability density functions of cement: (a) reference; (b) SiO_2; (c) SiO_2 + P; and (d) SiO_2@PEGMA.

https://doi.org/10.1021/acsomega.2c03202
ACS Omega 2022, 7, 24012−24019

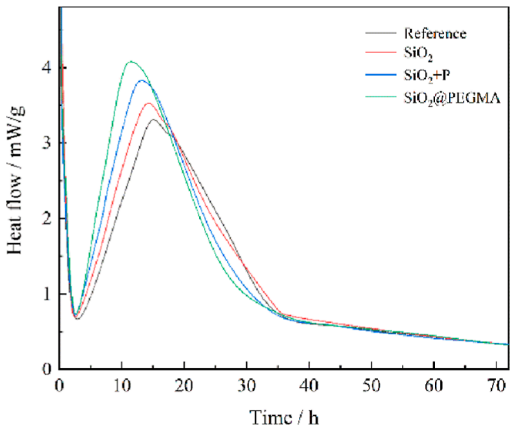

Figure 6. Head flow curves of four kinds of cement pastes.

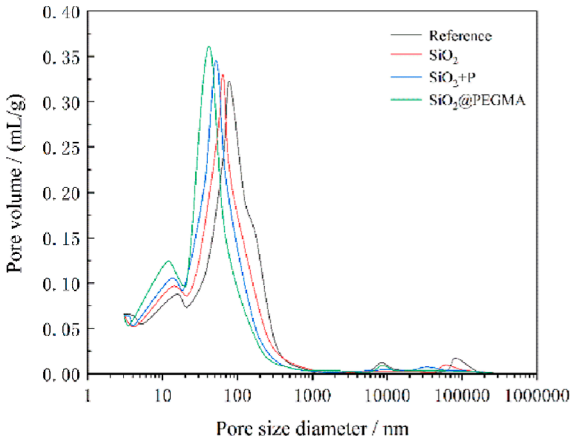

Figure 8. Pore size distribution of four kinds of cement samples.

3.7. Scanning Electron Micrograph Analysis. BES-SEM was used to investigate the polished surfaces of hardened cement pastes, as illustrated in Figure 7. The black, gray, and white regions represented porosity, hydration products, and unreacted cement particles. The results showed that compared with other control groups, SiO_2@PEGMA composites could appreciably reduce the number of unreacted cement particles and porosity while increasing the number of hydration products. Although superplasticizers could facilitate the dispersion stability of SiO_2 nanoparticles through electrostatic adsorption, it was challenging for the SiO_2 nanoparticles to be compatible with superplasticizers by physical blending, and SiO_2 nanoparticles were still easily agglomerated in cement pore solutions. At the same time, the core−shell structure of SiO_2@PEGMA composites could solve the above problems. This indicated that SiO_2@PEGMA composites could densify the microstructure of hardened cement pastes, which was beneficial to the compressive strength of oil well cement.

3.8. Pore Structure Analysis. The pore size distribution and total porosity of cement samples are illustrated in Figure 8 and Table 3, respectively. Compared with the reference sample, the pore size distribution curve of cement with additives moved toward the small pore, which indicated that the additives might improve the pore structure. Furthermore, the addition of SiO_2@PEGMA composites led to a reduction in the average pore diameter and total porosity of up to 12.5 nm and 16.8% compared with the reference, respectively, showing more effective results in improving the pore structure. SiO_2@PEGMA composites with the core−shell structure could significantly promote the hydration process through the seeding effect. In addition, the smaller SiO_2@PEGMA composites in cement pore solution could more easily fill spaces between cement grains during the plastic procedure and fill pores during the hardening step. Furthermore, SiO_2@PEGMA composites reacted with $Ca(OH)_2$ in the hydration product matrix to generate C−S−H by the pozzolanic effect, promoting the hydration process and resulting in a denser microstructure.

Table 3. Pore Structure Parameters of Cement Samples

cement samples	average pore diameter/nm	total porosity/%
reference	27.7	36.2
SiO_2	24.5	32.3
SiO_2 + P	20.6	26.5
SiO_2@PEGMA	15.2	19.4

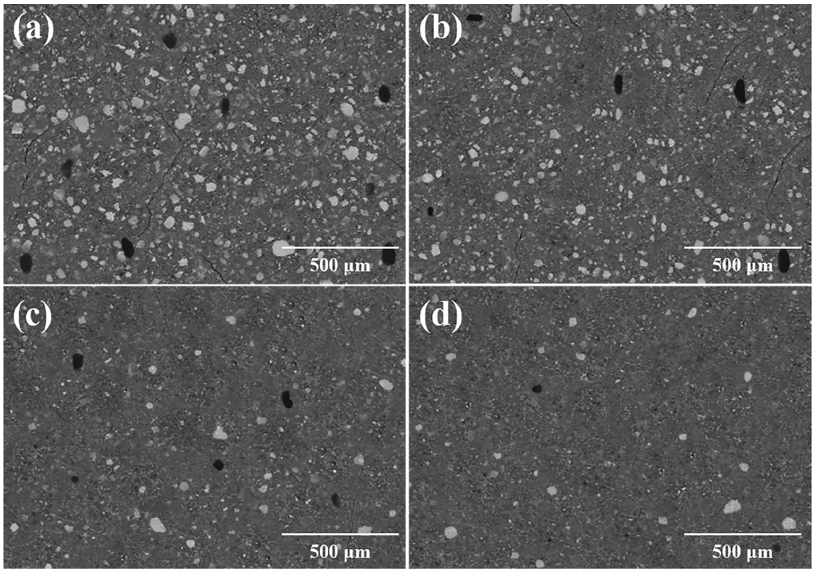

Figure 7. BES-SEM images: (a) reference cement; (b) SiO_2 cement; (c) SiO_2 + P cement; and (d) SiO_2@PEGMA cement.

https://doi.org/10.1021/acsomega.2c03202
ACS Omega 2022, 7, 24012−24019

4. CONCLUSIONS

In this paper, SiO_2@PEGMA composites with the core−shell structure were successfully synthesized via radical polymerization. The PEGMA grafted on the SiO_2 nanoparticles enabled SiO_2@PEGMA composites with excellent dispersion stability by steric hindrance repulsive force. Even in saturated calcium hydroxide solution, SiO_2@PEGMA composites showed no significant difference in the cumulative particle size distribution compared with SiO_2 nanoparticles. Among all cement samples, SiO_2@PEGMA composites had the strongest influence on enhancing the compressive strength of hardened cement pastes, which increased by 36.7% after curing for 28 d. The SiO_2@PEGMA composites could not only promote the hydration process through the seeding effect but also compact the microstructure by physical filling. The PEGMA shell of SiO_2@PEGMA composites significantly inhibited the agglomeration of SiO_2 nanoparticles, enabling them to effectively exert the seeding effect, physical filling, and pozzolanic activity to improve the mechanical properties of cement.

AUTHOR INFORMATION

Corresponding Authors

Gang Wang − *School of Chemistry, Guangdong University of Petrochemical Technology, Maoming 525000, China; Guangdong Provincial Key Laboratory of Petrochemical Pollution Process and Control, Guangdong University of Petrochemical Technology, Maoming 525000, China;* orcid.org/0000-0002-0299-2360; Email: g.wang@gdupt.edu.cn

Hua Tan − *School of Chemistry, Guangdong University of Petrochemical Technology, Maoming 525000, China;* orcid.org/0000-0002-0119-9985; Email: huatan@gdupt.edu.cn

Authors

Chunjing Lu − *School of Petroleum Engineering, Northeast Petroleum University, Daqing 163318, China*

Ao Sun − *Center of Chemistry for Frontier Technologies, Zhejiang University, Hangzhou 310058, China*

Complete contact information is available at: https://pubs.acs.org/10.1021/acsomega.2c03202

Notes

The authors declare no competing financial interest.

ACKNOWLEDGMENTS

Authors would like to thank the Guangdong Basic and Applied Basic Research Foundation (2020A1515110411) and the Projects of Talents Recruitment of Guangdong University of Petrochemical Technology (518161).

REFERENCES

(1) Bagheri, M.; Shariatipour, S. M.; Ganjian, E. A review of oil well cement alteration in CO_2-rich environments. *Constr. Build. Mater.* **2018**, *186*, 946−968.

(2) Ahmed, A.; Elkatatny, S.; Adjei, S.; Al-Majed, A. Influence of Weighting Materials on the Properties of Oil-Well Cement. *ACS Omega* **2020**, *5*, 27618−27625.

(3) Pang, X.; Qin, J.; Sun, L.; Zhang, G.; Wang, H. Long-term strength retrogression of silica-enriched oil well cement: A comprehensive multi-approach analysis. *Cem. Concr. Res.* **2021**, *144*, 106424.

(4) Adjei, S.; Elkatatny, S. Overview of the lightweight oil-well cement mechanical properties for shallow wells. *J. Pet. Sci. Eng.* **2021**, *198*, 108201.

(5) Plank, J.; Tiemeyer, C.; Bülichen, D.; Recalde Lummer, N. A review of synergistic and antagonistic effects between oilwell-cement additives. *SPE Drill. Completion* **2013**, *28*, 398−404.

(6) Soares, L. W. O.; Braga, R. M.; Freitas, J. C. O.; Ventura, R. A.; Pereira, D. S. S.; Melo, D. M. A. The effect of rice husk ash as pozzolan in addition to cement Portland class G for oil well cementing. *J. Pet. Sci. Eng.* **2015**, *131*, 80−85.

(7) Choolaei, M.; Rashidi, A. M.; Ardjmand, M.; Yadegari, A.; Soltanian, H. The effect of nanosilica on the physical properties of oil well cement. *Mater. Sci. Eng. A* **2012**, *538*, 288−294.

(8) Quercia, G.; Brouwers, H. J. H.; Garnier, A.; Luke, K. Influence of olivine nano-silica on hydration and performance of oil-well cement slurries. *Mater. Des.* **2016**, *96*, 162−170.

(9) Yang, Y.; Deng, Y. Mechanical properties of hybrid short fibers reinforced oil well cement by polyester fiber and calcium carbonate whisker. *Constr. Build. Mater.* **2018**, *182*, 258−272.

(10) Alsaba, M. T.; Al Dushaishi, M. F.; Abbas, A. K. A comprehensive review of nanoparticles applications in the oil and gas industry. *J. Pet. Explor. Prod. Technol.* **2020**, *10*, 1389−1399.

(11) Wakeel, S. A.; Němeček, J.; Li, L.; Xi, Y.; Hubler, M. The effect of introducing nanoparticles on the fracture toughness of well cement paste. *Int. J. Greenhouse Gas Control* **2019**, *84*, 147−153.

(12) Maagi, M. T.; Lupyana, S. D.; Gu, J. Effect of nano-SiO_2, nano-TiO_2 and nano-Al_2O_3 addition on fluid loss in oil-well cement slurry. *Int. J. Concr. Struct. Mater.* **2019**, *13*, 1−6.

(13) Jiang, T.; Geng, C.; Yao, X.; Song, W.; Dai, D.; Yang, T. Long-term thermal performance of oil well cement modified by silica flour with different particle sizes in HTHP environment. *Constr. Build. Mater.* **2021**, *296*, 123701.

(14) Pimenta Teixeira, K.; Perdigão Rocha, I.; De Sá Carneiro, L.; Flores, J.; Dauer, E.; Ghahremaninezhad, A. The effect of curing temperature on the properties of cement pastes modified with TiO_2 nanoparticles. *Materials* **2016**, *9*, 952.

(15) Vipulanandan, C.; Mohammed, A. Magnetic field strength and temperature effects on the behavior of oil well cement slurry modified with iron oxide nanoparticles and quantified with Vipulanandan models. *J. Test. Eval.* **2019**, *48*, 4516−4537.

(16) Barbhuiya, S.; Mukherjee, S.; Nikraz, H. Effects of nano-Al_2O_3 on early-age microstructural properties of cement paste. *Constr. Build. Mater.* **2014**, *52*, 189−193.

(17) Niu, X.-J.; Li, Q.-B.; Hu, Y.; Tan, Y.-S.; Liu, C.-F. Properties of cement-based materials incorporating nano-clay and calcined nano-clay: A review. *Constr. Build. Mater.* **2021**, *284*, 122820.

(18) Reches, Y.; Thomson, K.; Helbing, M.; Kosson, D. S.; Sanchez, F. Agglomeration and reactivity of nanoparticles of SiO_2, TiO_2, Al_2O_3, Fe_2O_3, and clays in cement pastes and effects on compressive strength at ambient and elevated temperatures. *Constr. Build. Mater.* **2018**, *167*, 860−873.

(19) Tariq, Z.; Murtaza, M.; Mahmoud, M. Effects of nanoclay and silica flour on the mechanical properties of class G cement. *ACS Omega* **2020**, *5*, 11643−11654.

(20) Qing, Y.; Zenan, Z.; Deyu, K.; Rongshen, C. Influence of nano-SiO_2 addition on properties of hardened cement paste as compared with silica fume. *Constr. Build. Mater.* **2007**, *21*, 539−545.

(21) Meng, T.; Hong, Y.; Wei, H.; Xu, Q. Effect of nano-SiO_2 with different particle size on the hydration kinetics of cement. *Thermochim. Acta* **2019**, *675*, 127−133.

(22) Stefanidou, M.; Papayianni, I. Influence of nano-SiO_2 on the Portland cement pastes. *Composites, Part B* **2012**, *43*, 2706−2710.

(23) Zhuang, C.; Chen, Y. The effect of nano-SiO_2 on concrete properties: A review. *Nanotechnol. Rev.* **2019**, *8*, 562−572.

(24) Tadano, T.; Zhu, R.; Muroga, Y.; Hoshi, T.; Sasaki, D.; Yano, S.; Sawaguchi, T. Molecular weight dependence of SiO_2 nanoparticle agglomeration behavior in monodisperse PMMA-SiO_2 hybrid suspension. *Chem. Lett.* **2014**, *43*, 705−707.

(25) Zapata, L. E.; Portela, G.; Suárez, O. M.; Carrasquillo, O. Rheological performance and compressive strength of superplasticized cementitious mixtures with micro/nano-SiO_2 additions. *Constr. Build. Mater.* **2013**, *41*, 708−716.
(26) Sarde, B.; Patil, Y. D. Recent research status on polymer composite used in concrete-an overview. *Mater. Today: Proc.* **2019**, *18*, 3780−3790.
(27) Flatt, R. J.; Houst, Y. F. A simplified view on chemical effects perturbing the action of superplasticizers. *Cem. Concr. Res.* **2001**, *31*, 1169−1176.
(28) Jansen, D.; Neubauer, J.; Goetz-Neunhoeffer, F.; Haerzschel, R.; Hergeth, W.-D. Change in reaction kinetics of a Portland cement caused by a superplasticizer-Calculation of heat flow curves from XRD data. *Cem. Concr. Res.* **2012**, *42*, 327−332.
(29) Sha, S.; Wang, M.; Shi, C.; Xiao, Y. Influence of the structures of polycarboxylate superplasticizer on its performance in cement-based materials-A review. *Constr. Build. Mater.* **2020**, *233*, 117257.
(30) Mallakpour, S.; Naghdi, M. Polymer/SiO_2 nanocomposites: Production and applications. *Prog. Mater. Sci.* **2018**, *97*, 409−447.
(31) Zhang, L.; Miao, X.; Kong, X.; Zhou, S. Retardation effect of PCE superplasticizers with different architectures and their impacts on early strength of cement mortar. *Cem. Concr. Compos.* **2019**, *104*, 103369.
(32) Pourhashem, S.; Saba, F.; Duan, J.; Rashidi, A.; Guan, F.; Nezhad, E. G.; Hou, B. Polymer/inorganic nanocomposite coatings with superior corrosion protection performance: A review. *J. Ind. Eng. Chem.* **2020**, *88*, 29−57.
(33) Hsissou, R.; Seghiri, R.; Benzekri, Z.; Hilali, M.; Rafik, M.; Elharfi, A. Polymer composite materials: A comprehensive review. *Compos. Struct.* **2021**, *262*, 113640.
(34) Kim, Y.-J.; Ha, S.-W.; Jeon, S.-M.; Yoo, D. W.; Chun, S.-H.; Sohn, B.-H.; Lee, J.-K. Fabrication of triacetylcellulose-SiO_2 nanocomposites by surface modification of silica nanoparticles. *Langmuir* **2010**, *26*, 7555−7560.
(35) Mallakpour, S.; Naghdi, M. Application of SiO_2 nanoparticles with double layer coverage consist of citric acid and l (+)-ascorbic acid for the production of poly (vinyl chloride)/SiO_2 nanocomposite films with enhanced optical and thermal properties. *Polym. Bull.* **2016**, *73*, 1701−1717.
(36) Huang, Q.; Liu, M.; Mao, L.; Xu, D.; Zeng, G.; Huang, H.; Jiang, R.; Deng, F.; Zhang, X.; Wei, Y. Surface functionalized SiO_2 nanoparticles with cationic polymers via the combination of mussel inspired chemistry and surface initiated atom transfer radical polymerization: Characterization and enhanced removal of organic dye. *J. Colloid Interface Sci.* **2017**, *499*, 170−179.
(37) Zhao, Y.; Chen, Z.; Zhu, X.; Möller, M. A facile one-step approach toward polymer@SiO_2 core-shell nanoparticles via a surfactant-free miniemulsion polymerization technique. *Macromolecules* **2016**, *49*, 1552−1562.
(38) Baek, Y.-M.; Shin, P.-S.; Kim, J.-H.; Park, H.-S.; DeVries, K. L.; Park, J.-M. Thermal transfer, interfacial, and mechanical properties of carbon fiber/polycarbonate-CNT composites using infrared thermography. *Polym. Test.* **2020**, *81*, 106247.
(39) Gao, H.; Wang, J.; Chen, X.; Wang, G.; Huang, X.; Li, A.; Dong, W. Nanoconfinement effects on thermal properties of nanoporous shape-stabilized composite PCMs: A review. *Nano Energy* **2018**, *53*, 769−797.
(40) Hsissou, R.; Berradi, M.; El Bouchti, M.; El Bachiri, A.; El Harfi, A. Synthesis characterization rheological and morphological study of a new epoxy resin pentaglycidyl ether pentaphenoxy of phosphorus and their composite (PGEPPP/MDA/PN). *Polym. Bull.* **2019**, *76*, 4859−4878.
(41) Su, N.; Miao, B.; Liu, F.-S. Effect of wash water and underground water on properties of concrete. *Cem. Concr. Res.* **2002**, *32*, 777−782.
(42) Long, W.-J.; Gu, Y.-c.; Xiao, B.-X.; Zhang, Q.-m.; Xing, F. Micro-mechanical properties and multi-scaled pore structure of graphene oxide cement paste: Synergistic application of nano-indentation, X-ray computed tomography, and SEM-EDS analysis. *Constr. Build. Mater.* **2018**, *179*, 661−674.
(43) Hu, C.; Li, Z. A review on the mechanical properties of cement-based materials measured by nanoindentation. *Constr. Build. Mater.* **2015**, *90*, 80−90.
(44) Reches, Y. Nanoparticles as concrete additives: Review and perspectives. *Constr. Build. Mater.* **2018**, *175*, 483−495.

https://doi.org/10.1021/acsomega.2c03202
ACS Omega 2022, 7, 24012−24019